Modulating oxygen vacancies in Sn-doped hematite film grown on silicon microwires for photoelectrochemical water oxidation

Zhongyuan Zhou,[a,b] Shaolong Wu,* [a,b] Linling Qin,[a,b] Liang Li,[a,b] Liujing Li[a,b] and Xiaofeng Li*[a,b]

[a] School of Optoelectronic Science and Engineering & Collaborative Innovation Center of Suzhou Nano Science and Technology, Soochow University, Suzhou 215006, China
[b] Key Lab of Advanced Optical Manufacturing Technologies of Jiangsu Province & Key Lab of Modern Optical Technologies of Education Ministry of China, Soochow University, Suzhou 215006, China
*Correspondence
Dr. Shaolong Wu; Prof. Xiaofeng Li
E-mail: shaolong_wu@suda.edu.cn; xfli@suda.edu.cn

Table S1 Reagents and related experimental materials are employed in the experiment.

Name	Molecular formula	Specification
Silicon	Si	N (100)，ρ (0.01-0.02 Ωcm)
Acetone	CH_3COCH_3	> 99.5%
Ethanol	CH_3CH_2OH	> 99.7%
Deionized water	H_2O	ρ ≥ 18.25 Ωm
Sulfuric acid	H_2SO_4	95.0% ~ 98.0%
Hydrogen peroxide	H_2O_2	AR，≥ 30%
Hydrofluoric acid	HF	AR，≥ 40%
Silver nitrate	$AgNO_3$	AR，≥ 99.8
Nitric acid	HNO_3	AR，65.0% ~ 68.0%
Ferric Nitrate	$Fe(NO_3)_3 \cdot 9H_2O$	AR, ≥ 99.99%
Stannic Chloridc	$SnCl_4 \cdot 5H_2O$	AR, ≥ 98%
Silica gel	—	NanDa 703
Developing solution	—	RZX-3038
Photoresist	—	RZJ-304

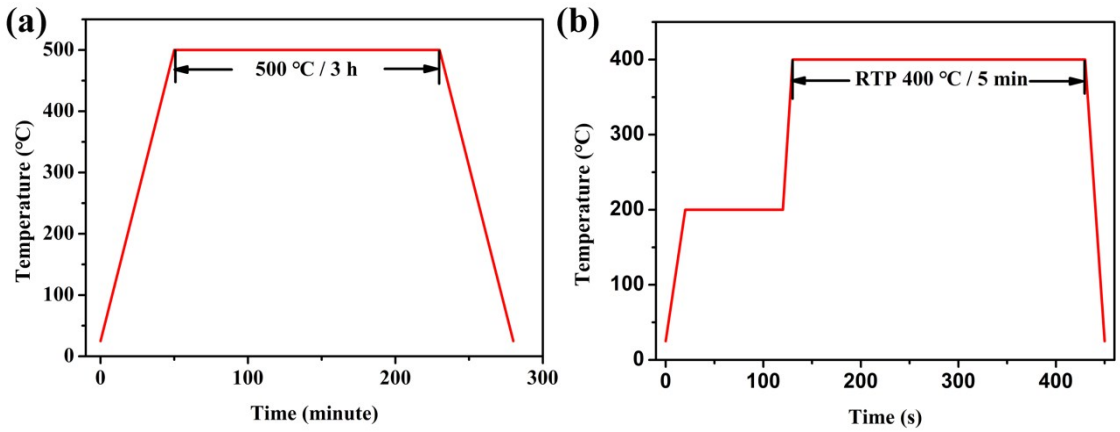

Fig. S1 (a) The normal thermal process for synthesizing the hematite; (b) the post-heating process with RTP for modifying the hematite.

Table S2. A comparison of the PEC performances between the typical hematite/silicon (and hematite) photoanodes in the related literatures and our present α-Fe_2O_3/SiMWs photoanode.

Photoanode	Film texture	Optimized sample (*J-V* curves)	$J_{ph@1.23V}$ U_{on}	Testing conditions (under AM 1.5G irradiation)	Key Method	Ref.
α-Fe_2O_3/n-SiNWs	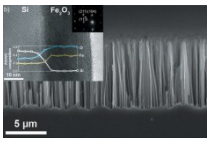	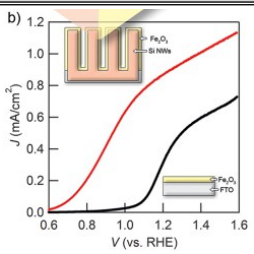	0.90 mA/cm^2 0.60 V_{RHE}	1 M NaOH	atomic layer deposition	[1]
α-Fe_2O_3/n-SiNWs	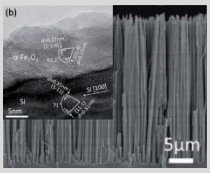	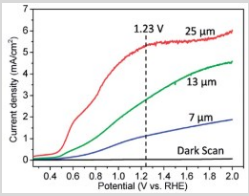	5.28 mA/cm^2 0.50 V_{RHE}	1 M NaOH (scan rate 50 mV/s) with magnetic stirring	deposition annealing	[2]
α-Fe_2O_3/n-SiNWs decorated with AuNPs	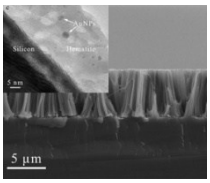	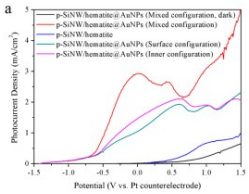	2.56 mA/cm^2 at 0 V vs. Pt mesh	1 M NaOH two-electrode cell	deposition annealing	[3]
Sn@α-Fe_2O_3/ SiMWs with RTP	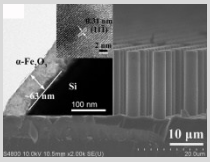	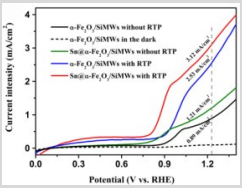	3.12 mA/cm^2 0.15 V_{RHE}	1 M NaOH (scan rate 20 mV/s)	Sn doping and RTP at 400 °C for 5 min	**This work**
Fe_2TiO_5/Fe_2O_3/ ITO/FTO with OER catalyst	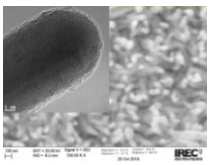	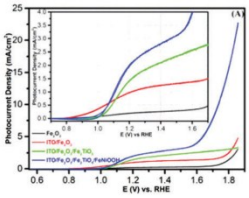	2.20 mA/cm^2 0.95 V_{RHE}	1 M NaOH purged with N_2 (scan rate 20 mV/s)	hydrothermal photoelectron-deposition, ALD, hydrothermal, sputtering	[4]
Pt-doped hematite with Co-Pi	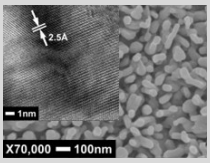	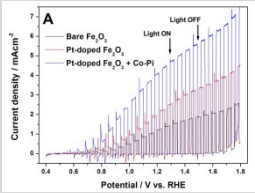	4.32 mA/cm^2 0.50 V_{RHE}	1 M NaOH	in-situ two-step annealing at 550 °C and 800 °C of FeOOH nanorods	[5]
α-Fe_2O_3/FTO	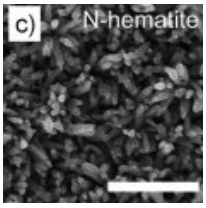	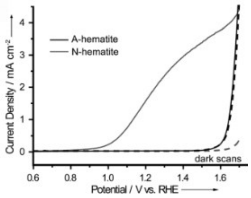	1.82 mA/cm^2 1.0 V_{RHE}	1 M NaOH (scan rate 10 mV/s)	sintered in an oxygen-deficient atmosphere (N_2+air) at 550 °C for 2 h	[6]

hematite nanoflake	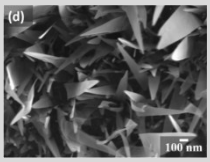	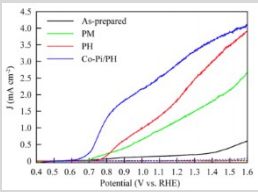	2.03 mA/cm^2 0.70 V_{RHE}	1 M NaOH under 500 W Xe lamp (285 mW/cm^2) illumination	plasma treatment at 18 W for 25 min	[7]
Sn@α-Fe_2O_3/FTO	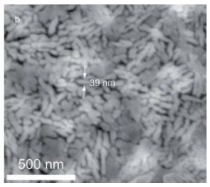	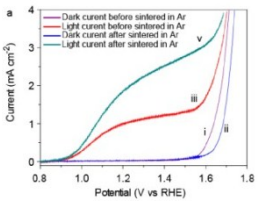	3.30 mA/cm^2 0.80 V_{RHE}	1 M NaOH	thermal post-treatment under Ar gas at 550 °C for 6 hours	[8]
α-Fe_2O_3/ITO	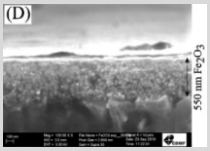	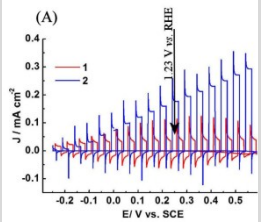	230 μA/cm^2 at 1.4 V_{RHE}	0.1 M NaOH electrolyte (scan rate 10 mV/s) under pulsed blue light	vacuum annealed at 400 °C for 2 hours	[9]

Table S3. A summary of the Mott-Schottky performance of the pristine SiMWs, the α-Fe_2O_3/FTO and the four modified α-Fe_2O_3/SiMWs hybrids.

Samples	N_D (cm^{-3})	U_{fb} (V_{RHE})
SiMWs	1.64×10^{18}	0.68
α-Fe_2O_3/FTO	2.09×10^{19}	0.53
α-Fe_2O_3/SiMWs	2.01×10^{18}	0.91
Sn@α-Fe_2O_3/SiMWs	3.98×10^{18}	0.89
α-Fe_2O_3/SiMWs with RTP	6.32×10^{18}	0.87
Sn@α-Fe_2O_3/SiMWs with RTP	1.92×10^{19}	0.84

Table S4. The fitting EIS data of the α-Fe_2O_3/SiMWs with various treatments based on equivalent circuits.

Sample	R_S(Ω)	R_{CT}(Ω)	C_{SC}(F)
α-Fe_2O_3/SiMWs	63.86	545.8	2.34×10^{-8}
Sn@α-Fe_2O_3/SiMWs	19.19	257	1.18×10^{-8}
α-Fe_2O_3/SiMWs with RTP	18.17	65.38	8.09×10^{-8}
Sn@α-Fe_2O_3/SiMWs with RTP	10.74	13.87	4.81×10^{-7}

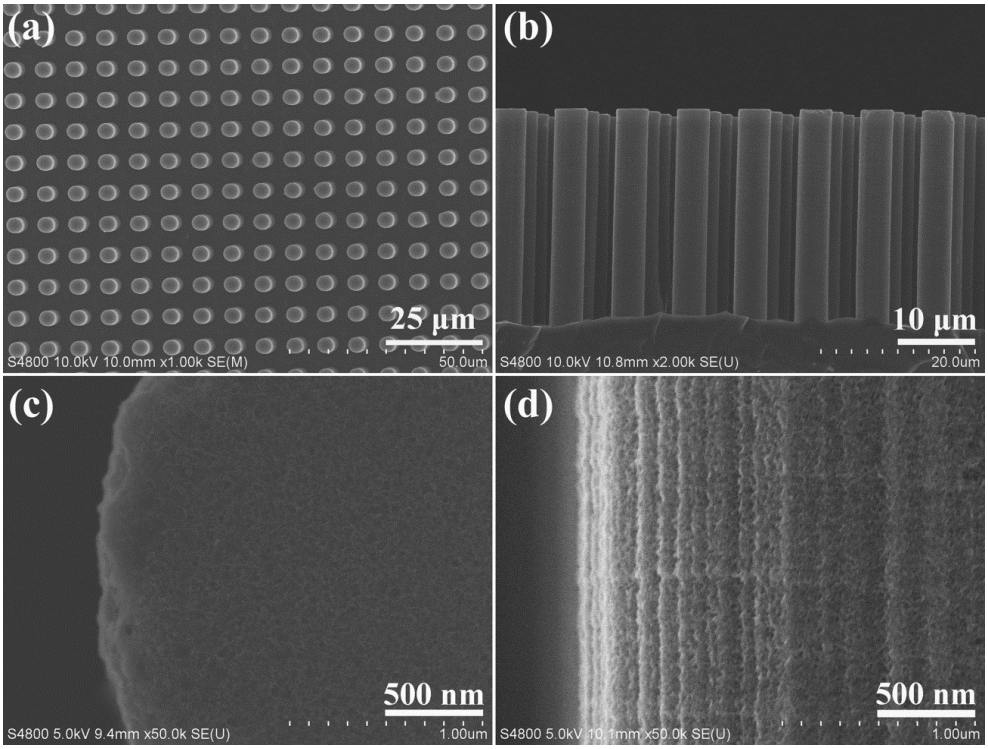

Fig. S2 (a–d) Typical SEM images of the freshly as-prepared SiMWs. (a) and (b) are the top view and cross-sectional image, respectively. (c) and (d) are the detail view of the top and the side, respectively.

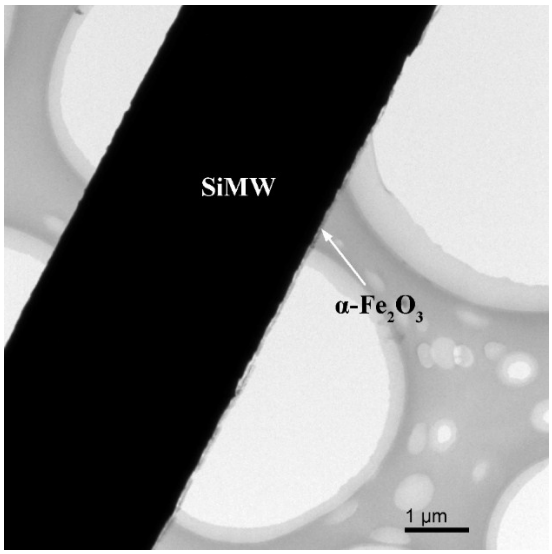

Fig. S3 TEM image of the uniform hematite film conformally grown on SiMWs.

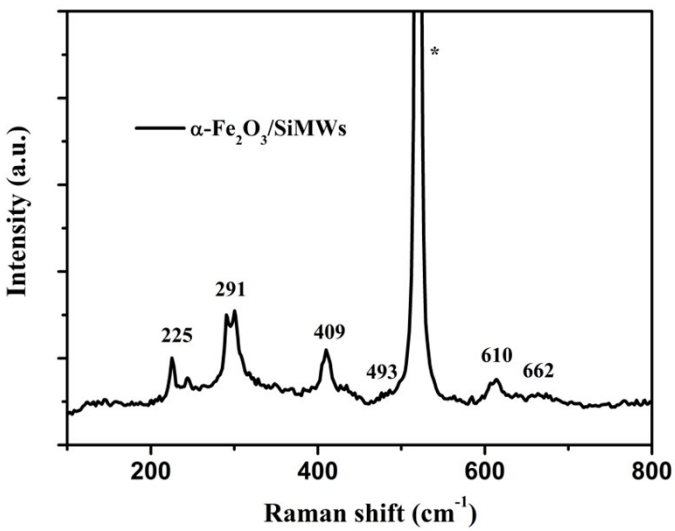

Fig. S4 Raman spectra of the α-Fe_2O_3/SiMWs. The five peaks (225 cm^{-1}, 291 cm^{-1}, 409 cm^{-1}, 498 cm^{-1} and 610 cm^{-1}) are correspond to the standard peaks of α-Fe_2O_3. The peak at 523 cm^{-1} is from the Si (distinguished by *), and the last peak at 662 cm^{-1} is assigned to the presence of Fe_3O_4, due to that FeO are not stable at room temperature.

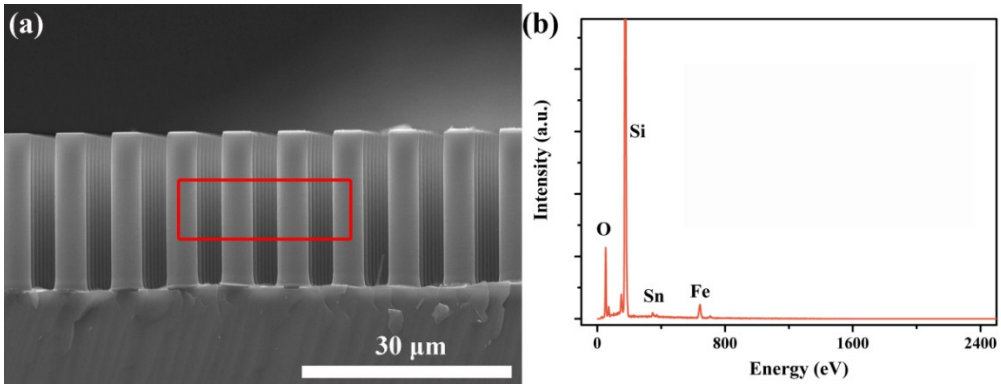

Fig. S5 SEM (a) and EDS spectrum (b) of the Sn@α-Fe_2O_3/SiMWs recorded in the red box in (a).

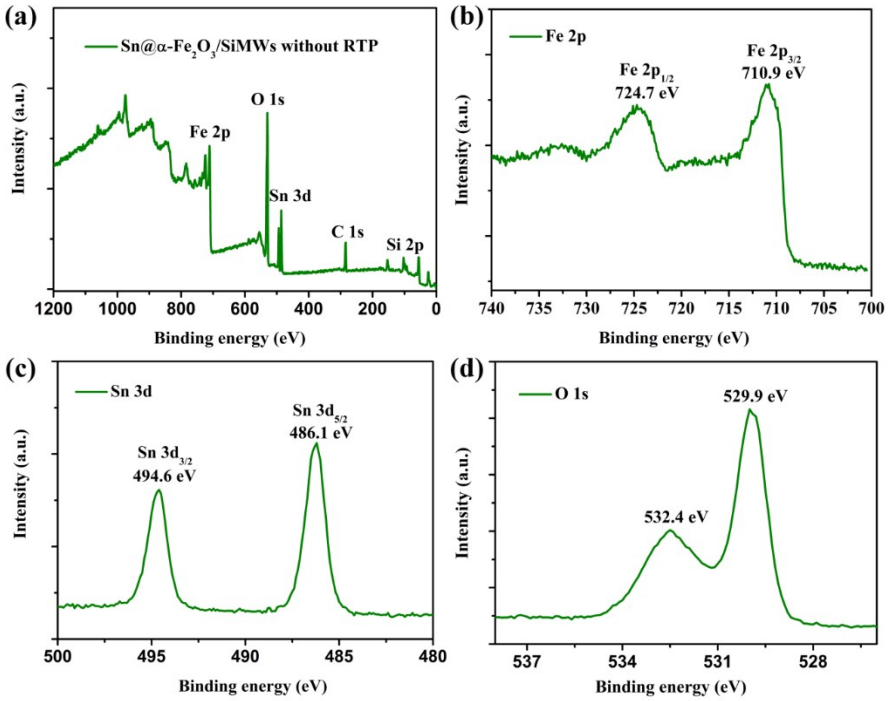

Fig. S6 XPS spectra of the Sn@α-Fe_2O_3/SiMWs. In (b), the peaks at 724.7 eV and 710.9 eV are ascribed to the Fe $2p_{1/2}$ and Fe $2p_{3/2}$, indicating the typical values of Fe^{3+} in Fe_2O_3. In (c) the Sn $3d_{5/2}$ (486.1 eV) and Sn $3d_{3/2}$ (494.6 eV) indicate that the Sn exists in the Sn@α-Fe_2O_3/SiMWs. In (d), two peaks at 529.9 eV and 532.4 eV are assigned to iron oxide lattice (Fe-O) and hydroxyl groups (Fe-OH adsorbed), respectively.

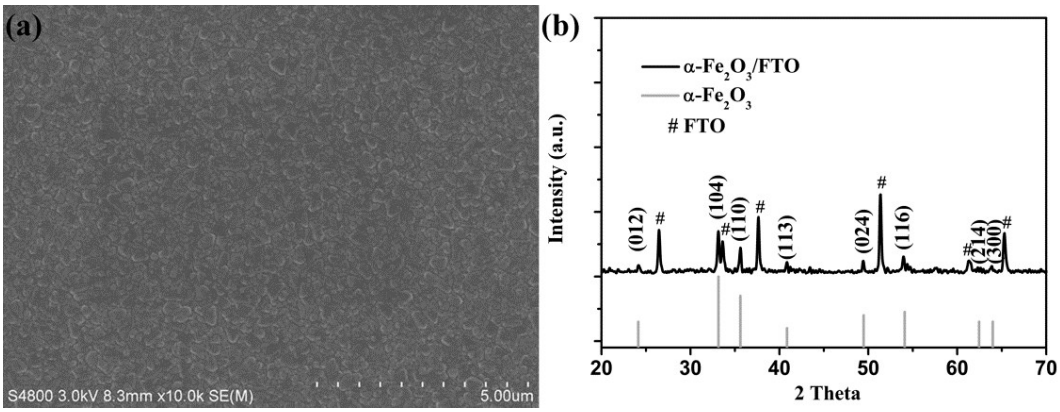

Fig. S7 SEM image of the α-Fe_2O_3 grown on the FTO substrate (a) and the corresponding XRD pattern (b).

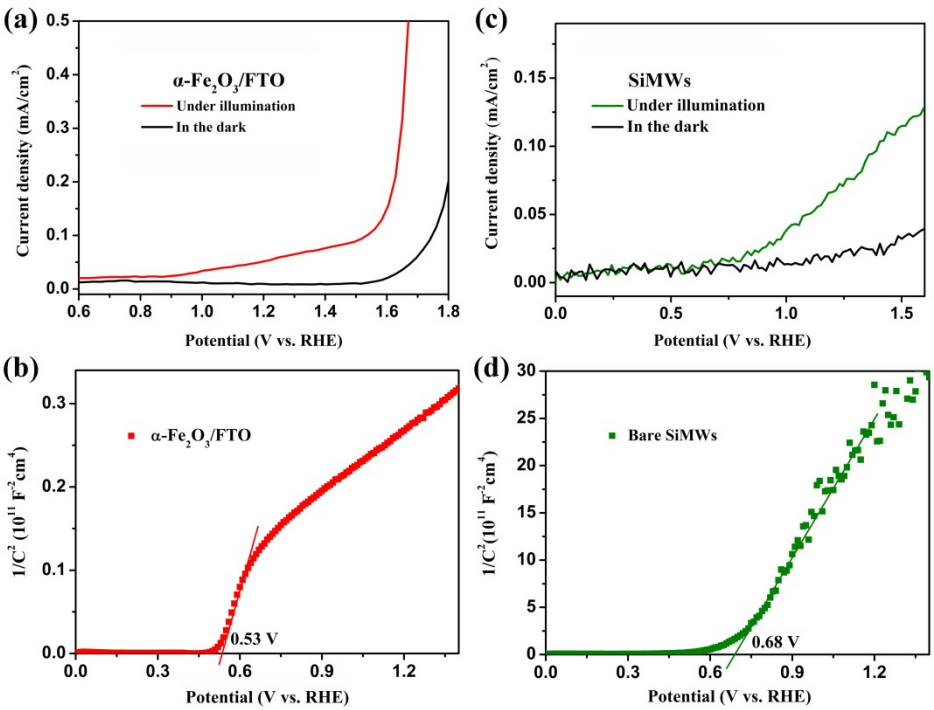

Fig. S8 Photoelectrochemical properties of the α-Fe_2O_3/FTO (a, b) and the bare SiMWs (c, d). (a and c) are the *J-V* curves. (b and d) are the Mott-Schottky plots.

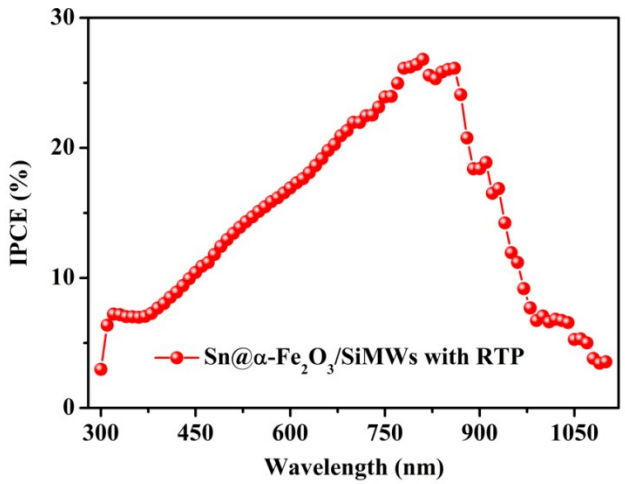

Fig. S9 IPCE spectra of the Sn@α-Fe_2O_3/SiMWs with RTP under 0.5 V bias between the photoanode and Pt electrode (i.e., the applied potential is calculated to be ~1.3 V_{RHE} according to the Nernst equation).

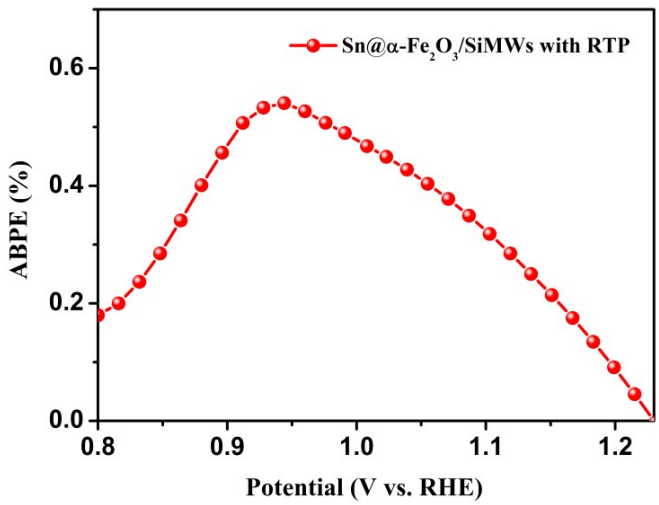

Fig. S10 The applied bias photon-to-current efficiency (ABPE) of the Sn@α-Fe_2O_3/SiMWs with RTP.

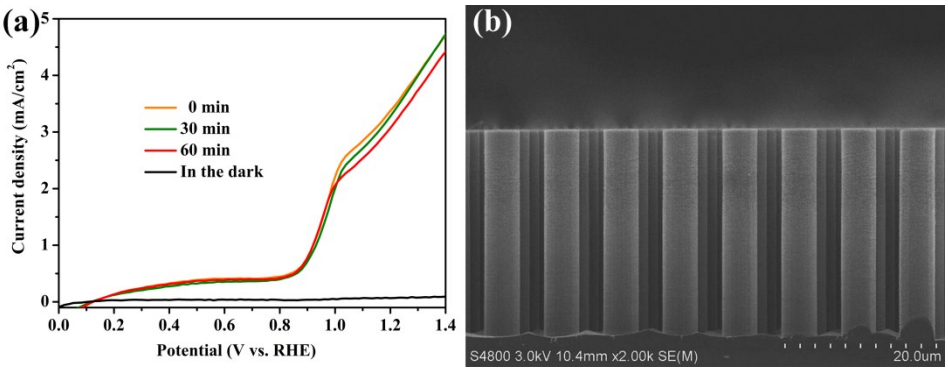

Fig. S11 (a) *J-V* curves of the Sn@α-Fe_2O_3/SiMWs with RTP after PEC measurement for different operation time; (b) SEM images of the Sn@α-Fe_2O_3/SiMWs with RTP after PEC testing for 1 h.

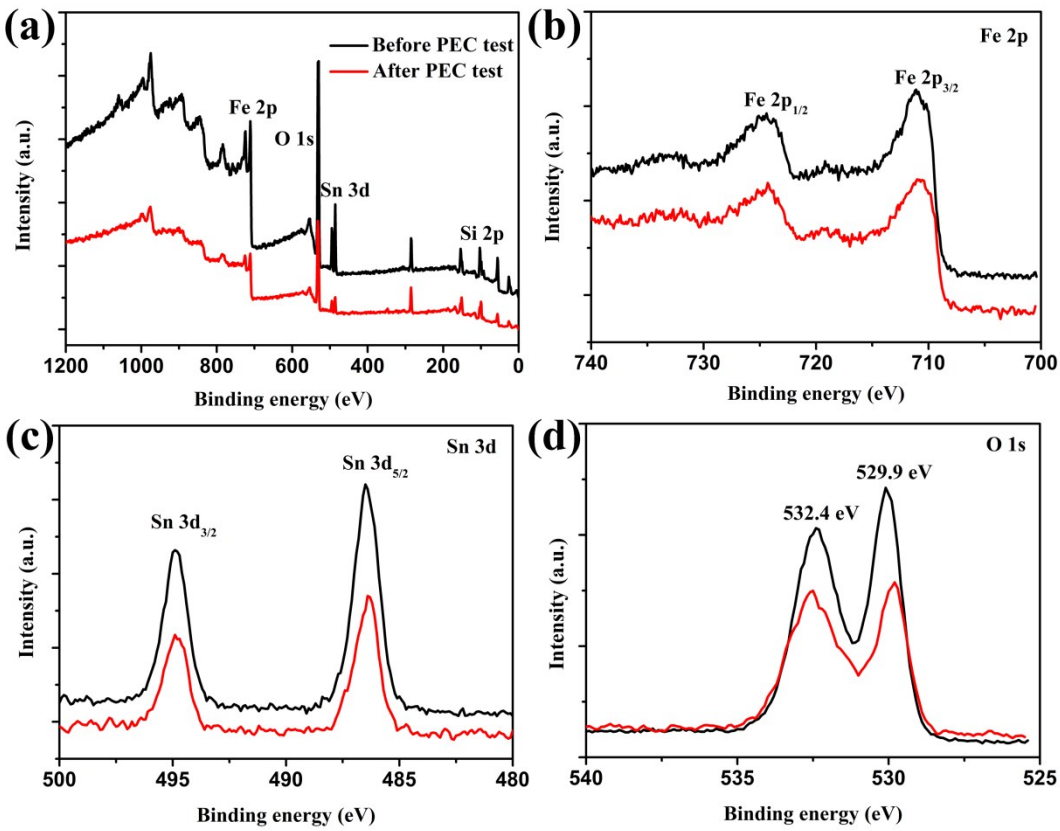

Fig. S12 XPS spectra of the Sn@α-Fe_2O_3/SiMWs with RTP before PEC test and after PEC test.

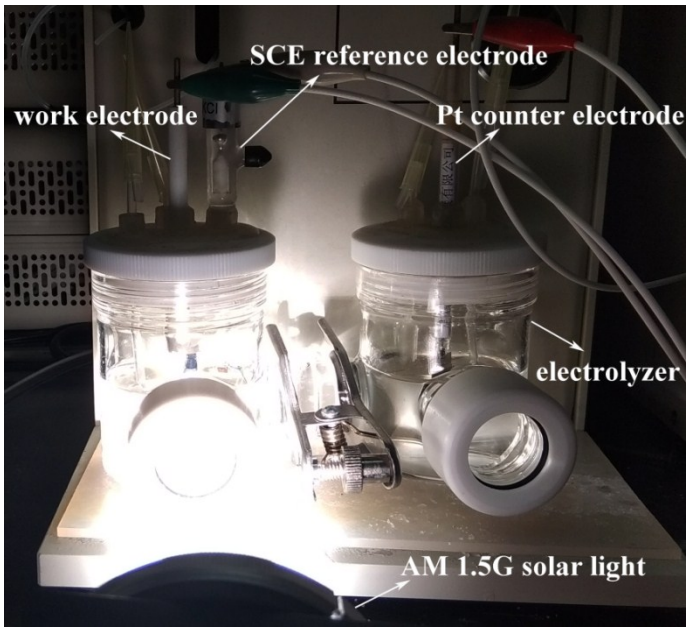

Fig. S13 The employed system for H_2 and O_2 evolution amount from a PEC cell.

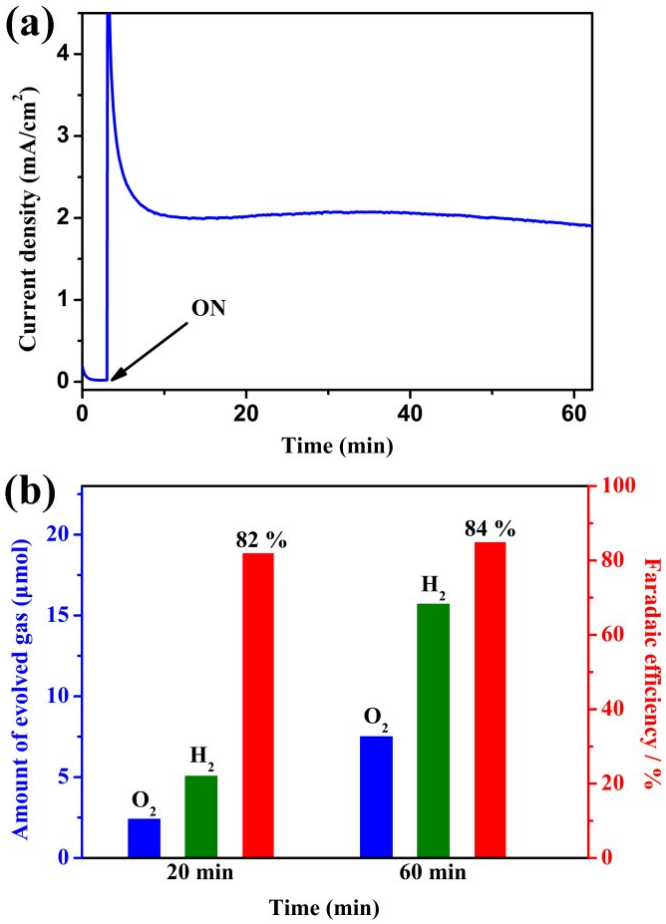

Fig. S14 (a) Photocurrent density vs. time (*I-t*) curve of the Sn@α-Fe_2O_3/SiMWs with RTP, the curve was obtained under simulated AM 1.5 G illumination at potential of 1.23 V vs. RHE in 1.0 M NaOH electrolyte. (b) Gas evolution amount and the calculated Faradaic efficiency.

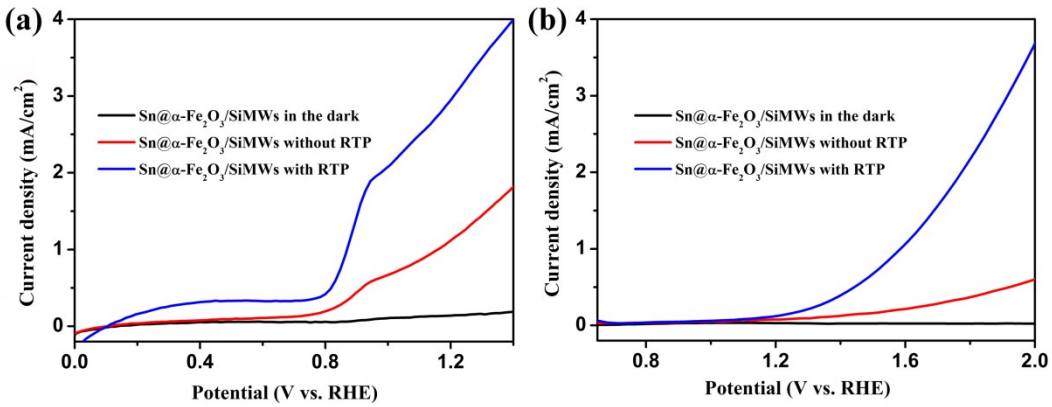

Fig. S15 *J-V* curves of the Sn@α-Fe_2O_3/SiMWs with RTP using (a) heavily n-doped (0.01–0.02 Ωcm) and (b) lightly n-doped Si (1–10 Ωcm) substrates.

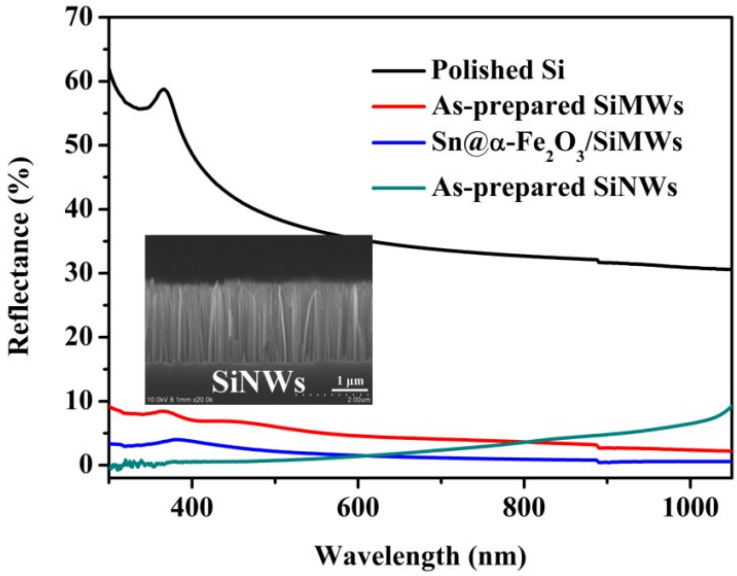

Fig. S16 Reflectance spectra of the polished Si, the bare SiMWs, the Sn@α-Fe_2O_3/SiMWs and the bare disordered Si nanowires (as shown in the inset SEM image) for using as a reference.

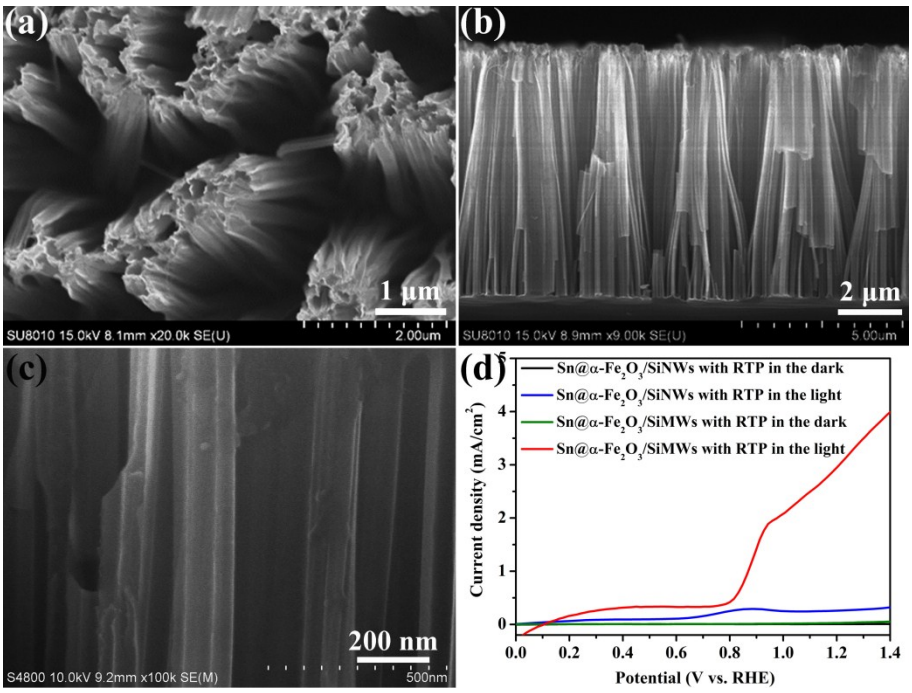

Fig. S17 SEM images of the prepared α-Fe_2O_3/SiNWs (a) top-view, (b) cross-section and (c) the detail view of the side; (d) *J-V* curves of the Sn@α-Fe_2O_3/SiMWs with RTP and the Sn@α-Fe_2O_3/SiNWs with RTP in the dark and under simulated AM 1.5G irradiation.

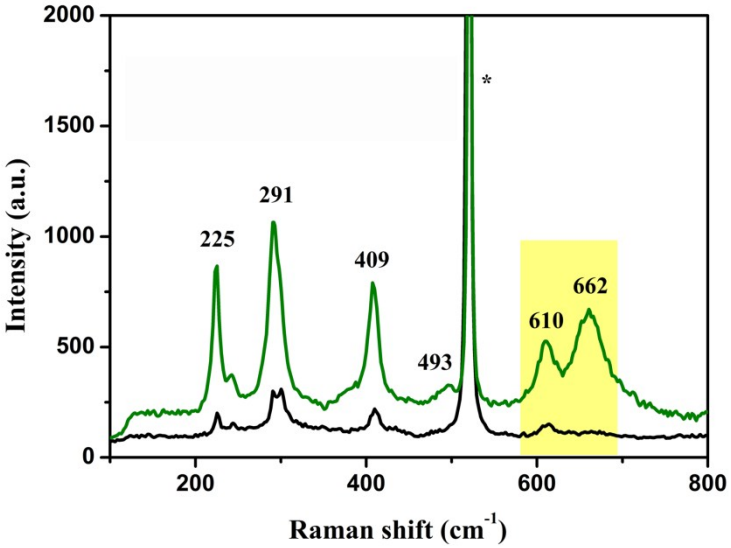

Fig. S18 The contrastive patterns of Raman of the Sn-doped and undoped α-Fe_2O_3/SiMWs without RTP (peaks indicated by * are from Si).

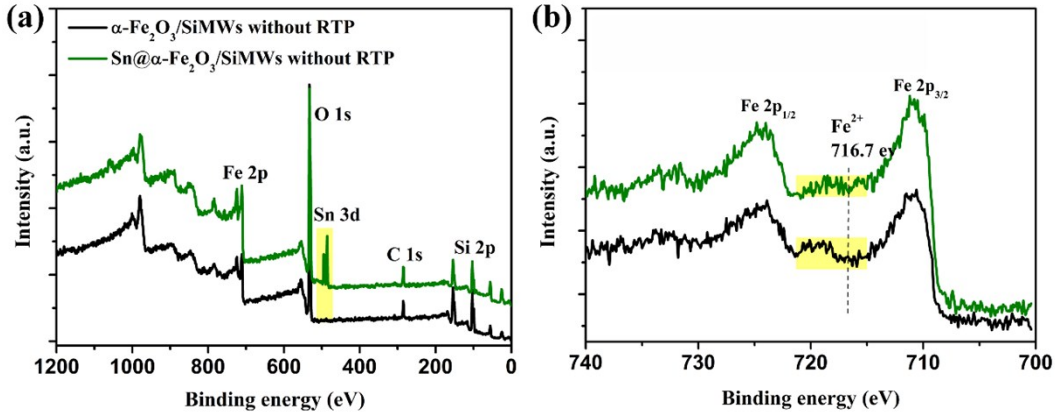

Fig. S19 The XPS contrastive plots of the Sn-doped and undoped α-Fe_2O_3/SiMWs photoanode.

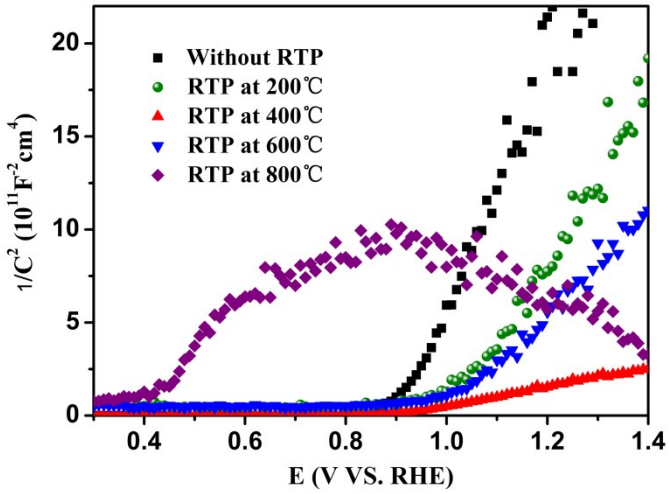

Fig. S20 Mott-Schottky plots of the Sn@α-Fe_2O_3/SiMWs with RTP at different temperatures.

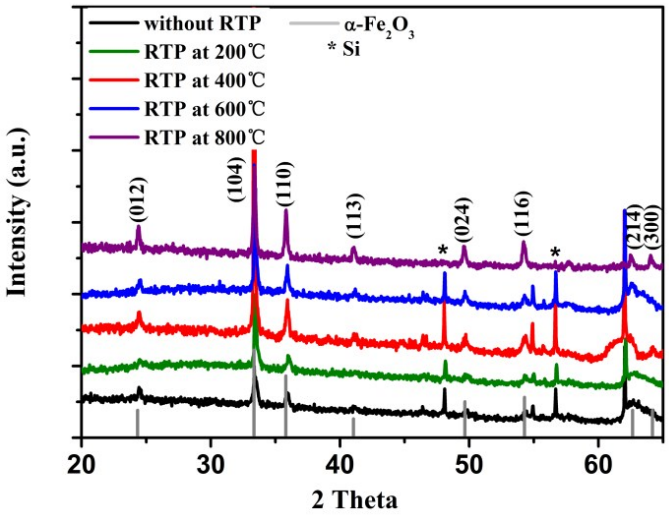

Fig. S21 The XRD patterns of the Sn@α-Fe_2O_3/SiMWs with RTP at different temperatures.

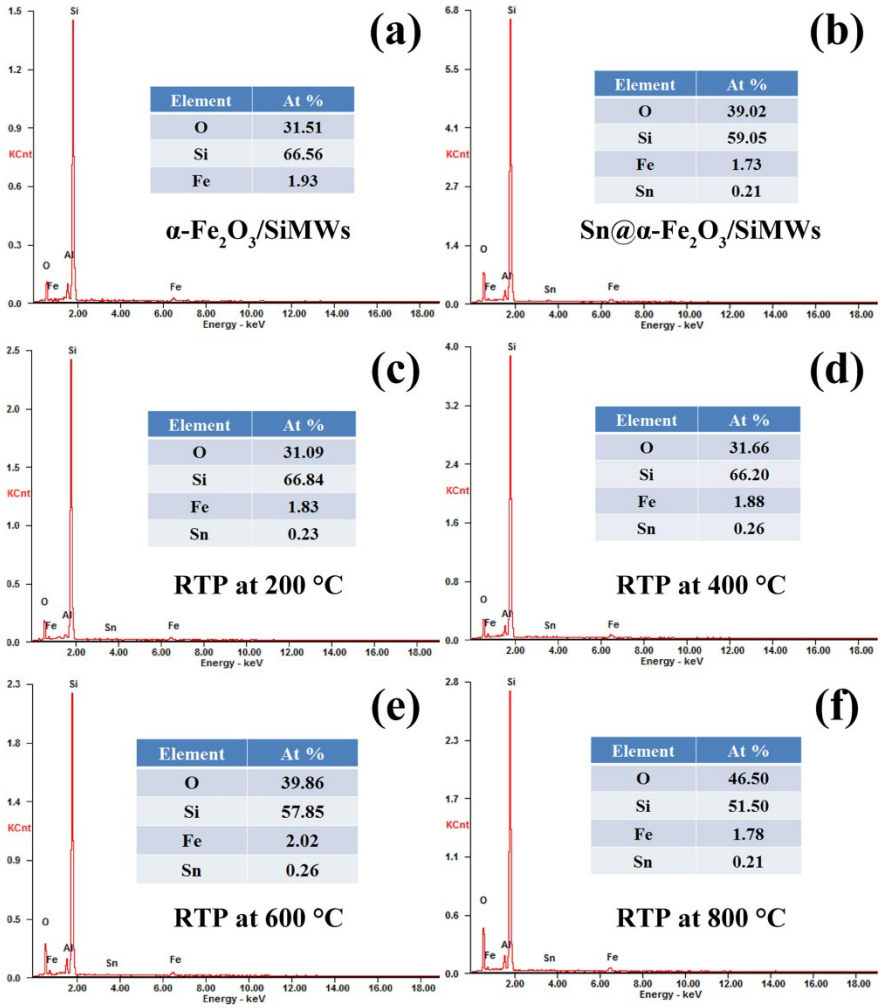

Fig. S22 EDS comparison for the undoped α-Fe_2O_3/SiMWs without RTP (a), the Sn-doped α-Fe_2O_3/SiMWs without RTP (b), and the Sn-doped α-Fe_2O_3/SiMWs with RTP at different temperatures (c–f), respectively.

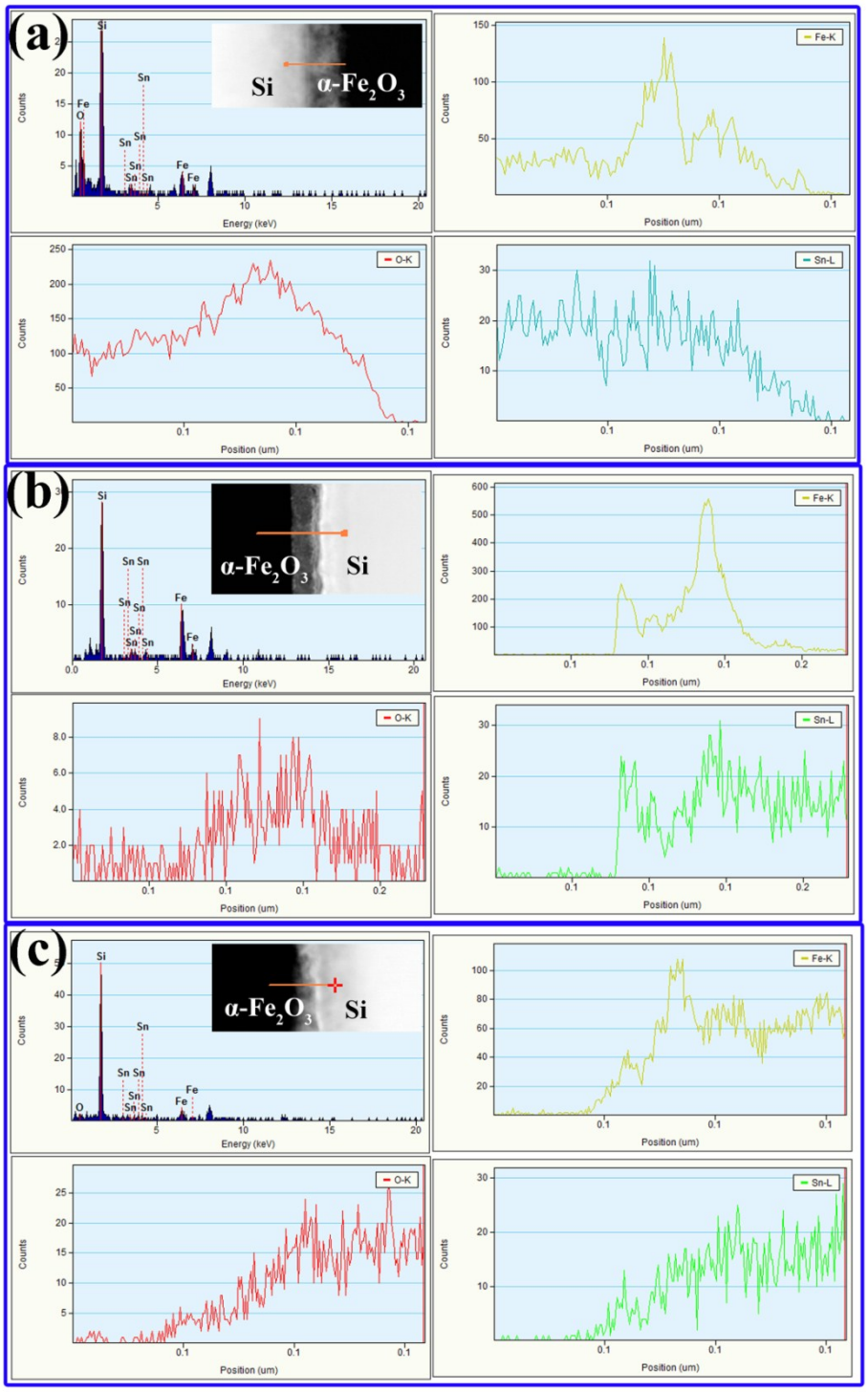

Fig. S23 EDS comparison for the Sn@α-Fe_2O_3/SiMWs without RTP (a), RTP at 400 °C (b) and RTP at 800 °C (c), respectively.

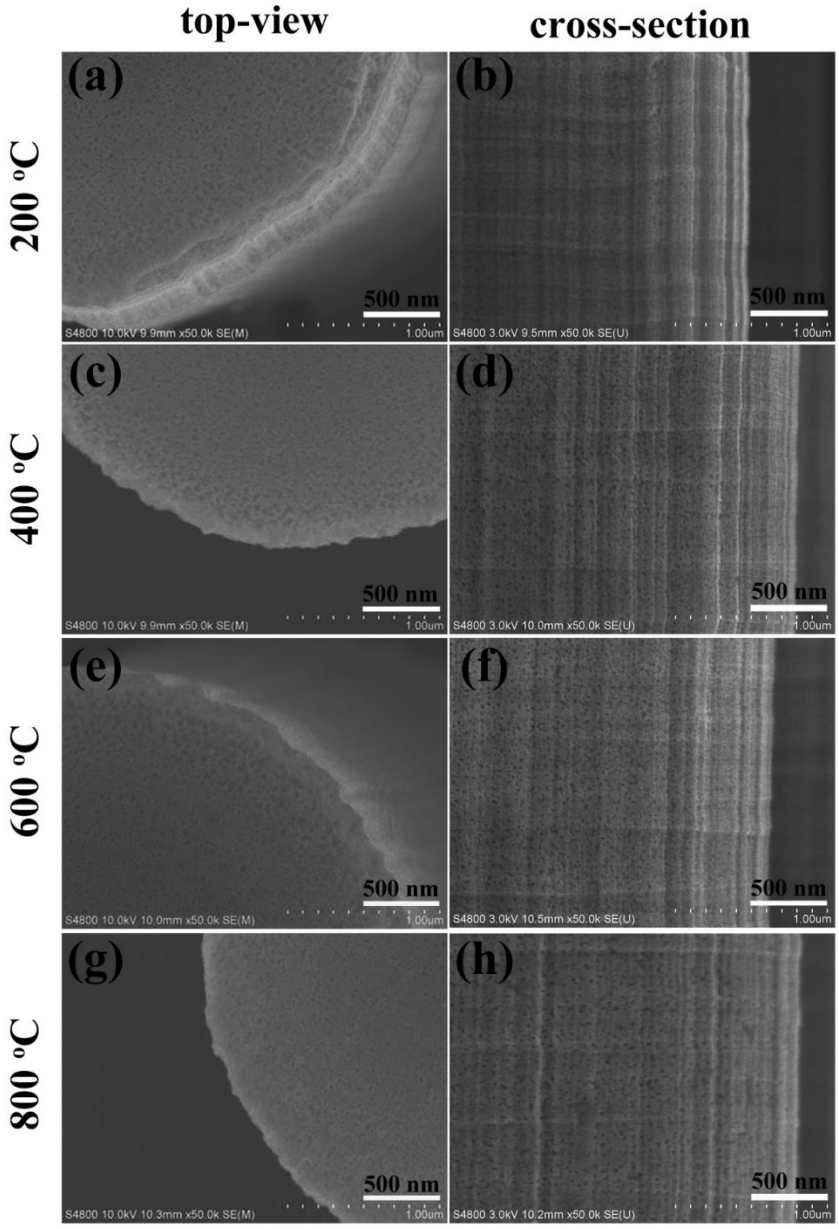

Fig. S24 The contrastive SEM images of the Sn@α-Fe_2O_3/SiMWs with RTP at different temperatures.

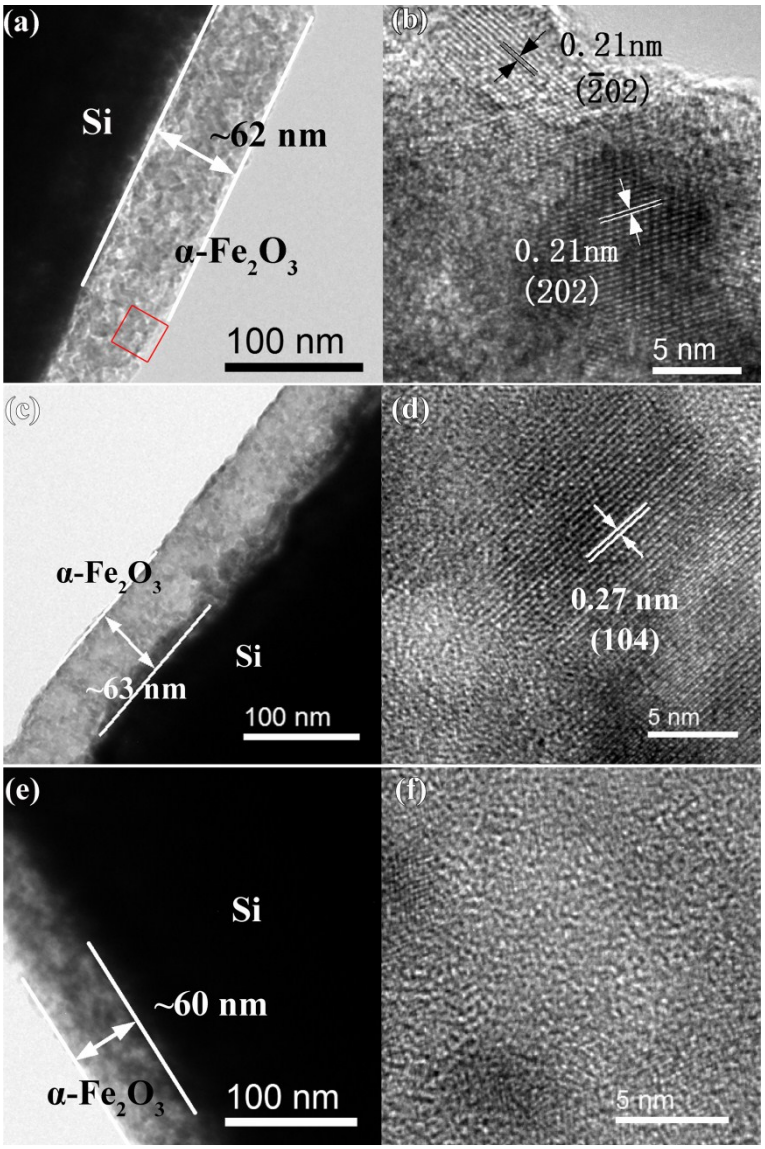

Fig. S25 HRTEM analysis of the synthesized Sn-doped α-Fe_2O_3 without RTP (a and b), with RTP at 400 °C (c and d) and RTP at 800 °C (e and f).

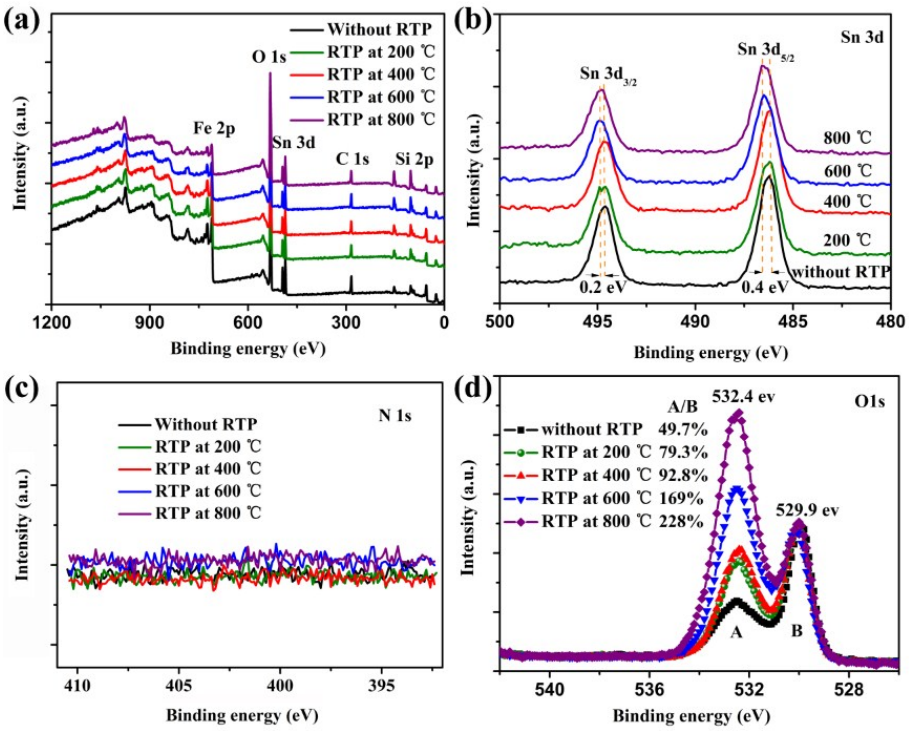

Fig. S26 The XPS spectra of (a) survey, (b) Sn 3d, (c) N 1s and (d) normalized XPS O1s peak of the Sn@α-Fe_2O_3/SiMWs with RTP at different temperatures.

References

[1] M. T. Mayer, C. Du and D. Wang, *J. Am. Chem. Soc.*, 2012, **134**, 12406–12409.

[2] X. Qi, G. She, X. Huang, T. Zhang, H. Wang, L. Mu and W. Shi, *Nanoscale*, 2014, **6**, 3182–3189.

[3] X. Wang, K.-Q. Peng, Y. Hu, F. Q. Zhang, B. Hu, L. Li, M. Wang, X. M. Meng and S. T. Lee, *Nano Lett.*, 2014, **14**, 18–23.

[4] P. Tang, H. Xie, C. Ros, L. Han, M. B. Peiro, Y. He, W. Kramer, A. P. Rodriguez, E. Saucedo, J. R. G. Mascaros, T. Andreu, J.R. Morante and J. Arbiol, *Energy Environ. Sci.*, 2017, **10**, 2124–2136.

[5] J. Y. Kim, G. Magesh, D. H. Youn, J. W. Jang, J. Kubota, K. Domen and J. S. Lee, *Sci. Rep.*, 2013, **3**, 2681.

[6] Y. Ling, G. Wang, J. Reddy, C. Wang, J. Zhang and Y. Li, *Angew. Chem. Int. Ed.*, 2012, **51**, 4074–4079.

[7] C. Zhu, C. Li, M. Zheng and J. J. Delaunay, *ACS Appl. Mater. Interfaces*, 2015, **7**, 22355–22363.

[8] J. J. Wang, Y. Hu, R. Toth, G.Fortunato and A. Braun, *J. Mater. Chem. A.*, 2016, **4**, 2821–2825.

[9] A. N. Bondarchuk, L. M. Peter, G. P. Kissling, E. Madrid, J. A. Aguilar-Martinez, Z. Rymansaib, P. Iravani, M. Gromboni, L. H. Mascaro, A. Walsh, F. Marken, *Appl. Catal. B-Environ.*, 2017, **211**, 289–295.